Efficient Access Control for Broadband Power Line Communications in Home Area Networks

Yinjia Huo, *Student Member, IEEE,* Gautham Prasad, *Student Member, IEEE,* Lutz Lampe, *Senior Member, IEEE,* and Victor C. M. Leung, *Fellow, IEEE*

***Abstract*—In this paper, we address the problem of improving the medium access control (MAC) layer efficiency in indoor broadband power line communication (BB-PLC) networks. Several overheads in the MAC layer, like random back-offs and collision recovery, degrade the MAC efficiency. To reduce these overheads, we apply in-band full-duplexing (IBFD), which enables medium-aware transmission at all the network nodes. Specifically, we propose two new schemes called contention-free pre-sensing and mutual preamble detection to minimize the time spent during contentions and collisions. Considering the non-idealities of IBFD, we analytically show the feasibility of our solutions. We further design a comprehensive simulation model with multiple priority data frames and Poisson network traffic arrival to emulate a real in-home network traffic. We then present numerical results for both the classical saturated network model and the comprehensive traffic model, to show through OMNeT++ simulations that our presented solutions achieve over 95% of the optimum MAC efficiency that can only be attained in the idealized case of no contentions or collisions.**

***Index Terms*—Power line communications, home area network, MAC efficiency, contention-free pre-sensing, mutual preamble detection.**

I. Introduction

BROADBAND Power Line Communication (BB-PLC) provides an attractive alternative for a backbone and/or stand-alone communication medium for home area networks (HANs) as it uses the existing in-home wiring infrastructure for high-speed and reliable data communications [2], [3]. Since the introduction of the 10-Mbps class BB-PLC products of HomePlug 1.0 [4], data rates provided by BB-PLC have increased multi-fold. Current HomePlug AV2 compliant devices use multiple wires available in most in-home wiring installations to achieve multiple-input multiple-output operation, and offer data rates of up to 2 Gbps [5]. The gigabit range of throughput and the widespread availability of access points (i.e., power outlets) render power lines as a favorable communication medium for HANs [6].

A. Background and State-of-the-art in BB-PLC

Despite the high data rate obtained in the physical (PHY) layer, it remains a challenge for the Medium Access Control (MAC) layer to translate this PHY data rate efficiently into MAC throughput. The cause for this can be understood by examining the channel access procedure followed in typical BB-PLC protocols. Carrier sense multiple access (CSMA) with collision avoidance (CA) is implemented as the primary medium access scheme in popular BB-PLC standards like HomePlug AV (HPAV) and IEEE 1901 [5], [7]. CSMA/CA uses a random back-off strategy to prevent collisions. When a collision nevertheless occurs, a relatively long time is spent on collision recovery [8]. These contentions and collision overheads lead to an inefficient MAC protocol, since no payload data is transferred over the medium during the random back-offs or the collision recovery phase.

A possible solution to avoid the lengthy collision recovery is to implement CSMA with collision detection (CD). Applying CSMA/CD on power lines has been considered infeasible as it requires network nodes to support a full-duplex operation [9, Ch. 5]. The recent introduction of in-band full-duplexing (IBFD) for BB-PLC enables network nodes to sense the medium while simultaneously transmitting data [10]. This inspires us to propose not only a practical CD scheme, similar to CSMA/CD in full-duplex wireless networks [11], [12], but also devise an IBFD-based method to eliminate the redundant back-off stages. Although CSMA/CD is also implemented in early Ethernet networks [13, Ch. 6], we face unique challenges in BB-PLC scenarios as explained in Section III and Section IV.

B. Related Works on CSMA/CD using IBFD

CSMA/CD was also considered infeasible in wireless networks when the network nodes were unable to transmit and receive signals simultaneously in the same band [14]. Pseudo-CSMA/CD procedures, like CSMA with collision notification (CN), were instead proposed as a middle-ground solution between CSMA/CA and CSMA/CD [14]. However, the introduction of IBFD has propelled feasible CSMA/CD methods to be proposed for wireless networks. The authors in [15], [16] used IBFD to enable the receiver node to continuously transmit acknowledgments as collision-free indicators while receiving the data payload. Such a scheme not only deprives an IBFD system of the bidirectional data payload transmission, but also potentially causes multiple false alarms in conditions of packet errors. Furthermore, it introduces additional power consumption at the destination node for the continuous acknowledgment transmission [17]. Alternative CSMA/CD techniques were proposed for wireless networks in [11], [12] to detect a collision at the transmitter by sensing the medium

The authors are with the Department of Electrical and Computer Engineering, The University of British Columbia, Vancouver, BC, Canada. Email: yortka@ece.ubc.ca, gauthamp@ece.ubc.ca.

A part of this work has been presented at the IEEE Global Communications Conference (GLOBECOM), Washington D.C., USA, December, 2016 [1].

This work was supported by funding from the National Natural Science Foundation of China (Grant No. 61671088) and the Natural Sciences and Engineering Research Council of Canada (NSERC).

during transmission without relying on the feedback from the destination node. However, [11], [12] provided analysis of CSMA/CD under the assumption of Rayleigh channel and a fixed self-interference cancellation performance. In contrast, we specify a complete detection and reaction procedure to realize CSMA/CD in BB-PLC networks through the IBFD detection of preamble symbols, and prove the feasibility of our solution by analytically deriving the detection error and false alarm rates under a worst-case power line attenuation condition. For our calculations, we use the self-interference cancellation performance reported in the literature [10], [18], which is shown to be dependent on the power line channel attenuation.

C. Contributions

In this paper, we exploit the medium-aware transmission enabled by IBFD to propose two novel techniques. First, we propose a contention free pre-sensing (CFP) scheme to eliminate the redundant back-off stages. In this scheme, we use the IBFD operation to enable network nodes to simultaneously transmit and sense for priority resolution symbols (PRSs) during the priority resolution procedure (PRP). This lets a network node identify a contention-free condition (CFC) where no other nodes transmit a MAC frame of the same or a higher priority. Under such a condition, we allow the node to skip the random back-off stage, and gain access to the power line medium immediately after the PRP. As a result, the redundant back-off stages can be eliminated, and the MAC efficiency can be improved.

Next, with the same underlying principle, we propose a second access control scheme, called mutual preamble detection (MPD), which, when combined with CFP, further increases the MAC efficiency. Using the IBFD operation, we enable network nodes to preempt and thus avoid possible future frame collisions by sensing the medium while transmitting preambles. In this way, we eliminate the lengthy recovery time associated with a frame collision. This is especially beneficial for future in-home PLC networks that are expected to often operate under a heavily loaded network condition with an increased frame collision rate.

To determine the applicability of our schemes in BB-PLC networks, we analytically derive closed-form expressions for the pertinent detection error and false alarm rates. We then use the self-interference cancellation gain values reported for IBFD BB-PLC systems under realistic in-home channel and noise scenarios [18], to prove that the worst-case probabilities of false alarms and detection errors for a wide-range of PLC channel conditions are near-zero.

Finally, we build a comprehensive in-home power line network simulation model with multiple priority data frames and Poisson network traffic arrival to emulate a real HAN traffic. Using both this model and the classical simplistic model with a single priority saturated network traffic, we perform network simulations using OMNeT++, and demonstrate that the MAC layer overheads caused by contentions and collisions are significantly reduced by applying our new schemes.

D. Outline

The rest of the paper is organized as follows. In Section II, we describe the functioning of the current HPAV MAC protocol, focusing on the aspects relevant to the schemes we propose. In Section III and Section IV, we improve the MAC efficiency by proposing our new CFP and MPD schemes. We provide numerical results in Section V, where we describe the adopted simulation models and present the OMNeT++ simulation results. In Section VI, we discuss the implementation costs associated with our proposed solutions, and their interoperability with legacy devices. Finally, we conclude this paper in Section VII.

Throughout this work, we consider the channel access procedure specified in the HPAV protocol [8]. However, due to the inherent upward and downward compatibility that HPAV provides, as well as the incorporation of an HPAV-like MAC protocol in the IEEE 1901 standard [19, Ch. 8] and the ITU-T G.hn standard [20, Ch. 12], all solutions that we propose in this paper can also be easily extended to these BB-PLC standards [21], [22].

II. Functioning of the HPAV MAC Layer

In this section, we briefly describe some aspects of HPAV MAC protocol [8] that we modify in Sections III and IV, and also define the MAC efficiency, which we intend to improve with our proposed access control schemes.

A. MAC Operation in CSMA/CA Mode

Fig. 1 shows the time line of a MAC frame transmission under a standard CSMA/CA operation. In the following, we introduce components of its operation, which are relevant to the schemes we propose.

1) Priority Resolution Procedure: A MAC frame transmission is initiated with a PRP. The HPAV protocol specifies four priority levels from 0 (lowest) to 3 (highest) that the network nodes can choose from using two priority bits. The priorities are resolved bit-by-bit starting with the slot for PRS_0, and followed by PRS_1, with PRS_0 indicating the most significant bit in the binary representation of the priority level. Nodes with the highest priority level in the network win the PRP, which ensures messages of higher priority levels always get transmitted before those of lower priority levels [8, Ch. 3].

2) Collision Avoidance: Collision avoidance in CSMA/CA is realized through the random back-off mechanism. Nodes winning the PRP, or recovering from a collision, participate in the back-off stage, which consists of a variable number of back-off time slots of equal time intervals. At each back-off time slot, the back-off counter (BC) of a participating node is decreased by one. Upon arriving at $\text{BC} = 0$, a preamble is transmitted by this node in the subsequent back-off time slot. The nodes transmitting a preamble gain access to the channel and then transmit a frame control (FC) message of type start-of-frame (SOF), followed by the data payload [23].

3) Collision in the Network: Despite the precautions taken to avoid collisions, CSMA/CA does not guarantee collision-free transmission, especially with increased number of contending nodes [24]. A collision in the network node occurs

This article has been accepted for publication in a future issue of this journal, but has not been fully edited. Content may change prior to final publication. Citation information: DOI 10.1109/TCOMM.2017.2749398, IEEE Transactions on Communications

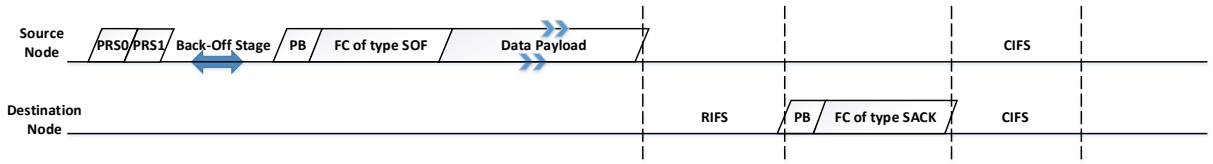

Fig. 1. Time line of an HPAV MAC frame transmission in CSMA/CA mode. (PB = Preamble)

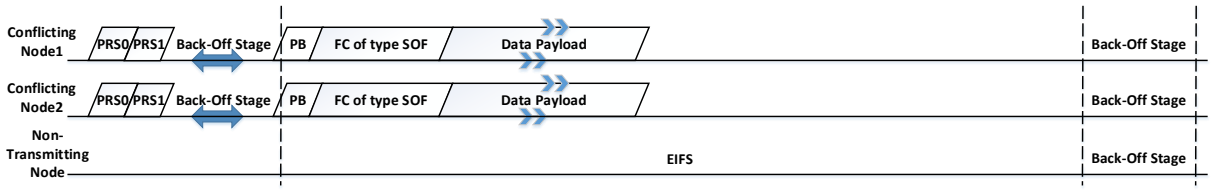

Fig. 2. Time line of a MAC frame transmission in case of a collision.

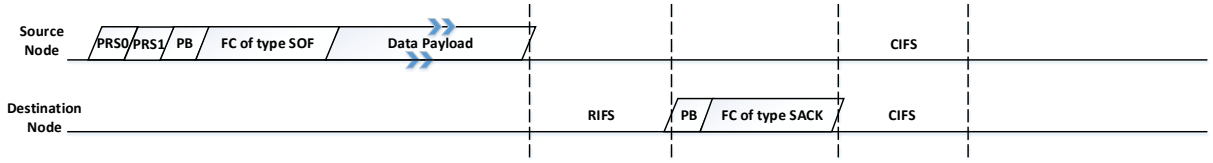

Fig. 3. Time line of a MAC frame transmission with CFP when a CFC successfully detected.

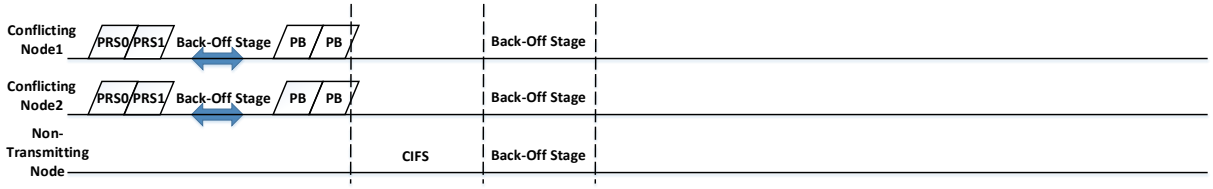

Fig. 4. Time line of a MAC frame transmission in case of a collision with the deployment of MPD.

when multiple nodes simultaneously transmit the preamble signal in a back-off time slot to gain access to the channel. A collision is determined at a network node if the node does not receive a selective acknowledgment (SACK) frame before the extended inter-frame space (EIFS) timer expires, as shown in Fig. 2.

4) Collision Recovery: Nodes recover from a collision immediately after the EIFS timer expires, and starts to back-off regardless of the priority level of the transmitting MAC frames. This operation is illustrated in Fig. 2. The EIFS has a duration of

$$t_{\mathsf{EIFS}} = 2t_{\mathrm{p}} + 2t_{\mathsf{FC}} + \mathsf{MaxFL} + t_{\mathsf{RIFS}} + t_{\mathsf{CIFS}}, \qquad (1)$$

where t_{p}, t_{FC}, MaxFL, t_{RIFS}, and t_{CIFS} are the time intervals of the preamble, the FC, the maximum time interval of the data payload, the response inter-frame space (RIFS), and the contention inter-frame space (CIFS), respectively. EIFS is therefore lengthy, and renders a collision very costly to recover from.

B. MAC Efficiency

As shown in Fig. 1, a data payload is only transmitted in the time interval following the SOF transmission. All other time intervals are overheads that impede the ability of the MAC layer to efficiently translate PHY data rate into the MAC throughput. To quantify this cross-layer throughput transfer, we define the MAC efficiency as the portion of time utilized by the MAC layer to transmit the data payloads, which is also referred to in the literature as the normalized throughput to evaluate the performance of a MAC protocol [25], [26].

For N collision-free frame transmissions over a time duration T, we define the MAC efficiency as

$$\eta \triangleq \frac{1}{T}\sum_{i=1}^{N} t_i, \qquad (2)$$

where t_i indicates the data payload interval of the ith frame, which is dependent on the traffic demands of the transmission station as well as the data payload PHY transmission rate, and is limited by MaxFL.

To determine the extent to which η can be improved, the ideal maximum MAC efficiency under CSMA operation can be computed under the condition that a network node continuously transmits frames of maximum length without incurring a collision, or back-off[1]. Under such conditions, each data payload is of the maximum time interval MaxFL, and each MAC frame shown in Fig. 1 is of an identical duration of $2t_{\mathrm{SLOT}} + t_{\mathrm{p}} + t_{\mathsf{FC}} + \mathsf{MaxFL} + t_{\mathsf{RIFS}} + t_{\mathrm{p}} + t_{\mathsf{FC}} + t_{\mathsf{CIFS}} = 2t_{\mathrm{SLOT}} + t_{\mathsf{EIFS}}$, where $2t_{\mathrm{SLOT}}$ is the time interval for two PRSs. Thus, the maximum MAC efficiency can be expressed as

$$\eta_{\max} = \frac{\mathsf{MaxFL}}{2t_{\mathrm{SLOT}} + t_{\mathsf{EIFS}}}. \tag{3}$$

With the objective of enhancing practical values of η as close as possible to $\eta_{\max}$, we attempt to reduce the MAC overheads caused by contentions and collisions, by proposing two new access control schemes in the following two sections.

III. Contention Free Pre-sensing

In this section, we propose our first scheme called CFP to detect a CFC during the PRP.

A. Network Operation with CFP

Recall that a CFC at a node is a condition where no other network node transmits a MAC frame of the same or a higher priority. To detect a CFC, we enable network nodes with the IBFD operation, and allow them to detect the PRS transmitted by other nodes while transmitting a PRS themselves. If a node does not detect any other PRS signals during its transmission, it identifies the channel to be contention-free, i.e., detects the presence of a CFC. In case a CFC is detected, as shown in Fig. 3, we skip the random back-off stage that traditionally follows the PRP, and let the source node transmit a preamble signal to gain access to the power line medium immediately after the PRP. Due to this, we observe from Figs. 1 and 3 that we save a time duration of up to $\mathsf{CW}_{\max} \cdot t_{\mathrm{SLOT}}$, which is otherwise wasted for a redundant back-off. $\mathsf{CW}_{\max}$ indicates the maximum contention window size.

B. Detecting CFC using IBFD CFP

Consider a network of K nodes, where N of those nodes contend to transmit a frame, with priority level p_n associated with each of the $n = 1, 2, ..., N$ nodes. A CFC occurs when only one of the N nodes transmits a message of the maximum priority level of all transmitting nodes, $\max(p_n)$, with $0 < \max(p_n) \leq p_{\mathrm{std}}$, where $p_{\mathrm{std}} = 2^m - 1$ $(m \in \mathbb{Z}^+)$ is the highest supported priority level of a message in the operating standard. For example, in the IEEE 1901 and HPAV standards, $m = 2$. In order to provide upward compatibility for future standards that may decide to support a greater number of priority levels to effectively serve traffic of varied nature, we present an analysis of our proposed CFP procedure for general m.

[1]For the sake of simplicity, we ignore the bursting and inverse bursting procedure specified in the HPAV protocol for this computation, without any adverse effects on our proposed solution. Results obtained in this paper can be easily extended to cases with bursting.

We define that a p_x-CFC occurs when only one network node transmits a message with $\max(p_n) = p_x$. Our CFP scheme is aimed to successfully detect such p_x-CFCs, for all $0 < p_x \leq p_{\mathrm{std}}$. Every priority level p_n can be expressed as

$$p_n = \sum_{i=0}^{m-1} 2^{m-1-i} \chi_i, \tag{4}$$

where $\chi_i \in \{0, 1\}$ is the binary value of the ith PRS, PRS_i, i.e., $\chi_i = 1$ when a PRS_i is transmitted by the node and $\chi_i = 0$ otherwise. The priority levels are resolved bit-by-bit through the m priority bits from PRS_0 to PRS_{m-1}, with the most significant bit, χ_0, transmitted first as PRS_0. During the PRP, a node of priority p_n transmits the PRS signal in PRS_i $(0 \leq i \leq m-1)$ if and only if $\chi_i = 1$.

Every p_n $(p_n \neq 0)$ is associated with a slot position $\bar{j_n}$, for which $\chi_{\bar{j_n}} = 1$ while $\chi_{j_n} = 0,\ \forall j_n > \bar{j_n}$. That is, $\chi_{\bar{j_n}}$ is the least significant 'bit 1' in the binary notation of p_n. With an intention to preserve the legacy PRP and introduce CFP as an add-on feature, we compel the nth network node with priority p_n to perform CFP only at $\mathsf{PRS}_{\bar{j_n}}$, when it has won all previous PRSs. If the node loses the PRP before $\mathsf{PRS}_{\bar{j_n}}$, it resigns from the PRP contention as per the legacy PRP, and therefore does not proceed to perform CFP.

When the node has won in all the previous priority resolution slots, it transmits a PRS at $\mathsf{PRS}_{\bar{j_n}}$, and so will any other node with the same or a higher priority level. Therefore, if the nth node detects another PRS transmitted at $\mathsf{PRS}_{\bar{j_n}}$, it deduces the presence of other node(s) of either the same or a higher priority level. In either case, the nth node deduces a non-CFC. However, if it does not detect any PRS in $\mathsf{PRS}_{\bar{j_n}}$, it deduces an absence of any other node with the same or a higher priority level. In such a CFC, the node skips the following back-off stage as described in Section III-A. This way, we ensure that the CFP procedure does not interfere with the conventional PRP, and is only a supplementary feature introduced to eliminate the redundant back-off stage under CFC.

The successful detection of a CFC is dependent on the extent of self-interference cancellation achieved by the IBFD solution. A non-ideal self-interference cancellation in IBFD could subject CFP to detection failure or false alarms. In the following, we analytically compute the probabilities of detection errors and false alarms using realistic self-interference cancellation gain values reported in [18].

C. Detection Error and False Alarm Rates

We denote the false alarm and detection error rates of the CFP at a network node as P_{FA} and P_{DE}, respectively. To aid our derivations, we define the following three events at a given network node.

- E_0: The node transmits a PRS.
- E_1: The node detects the presence of at least one PRS signal transmitted by another node in the network.
- E_2: At least one node other than the considered node actually transmits a PRS.

A false alarm occurs at a PRS transmitting node when it detects the presence of a PRS while no network nodes have

This article has been accepted for publication in a future issue of this journal, but has not been fully edited. Content may change prior to final publication. Citation information: DOI 10.1109/TCOMM.2017.2749398, IEEE Transactions on Communications

actually transmitted a signal. Similarly, a PRS transmitting node is subject to detection errors when it fails to detect a PRS signal when at least one other network node has transmitted the signal. Therefore, we formulate the error probabilities as

$$P_{\mathsf{FA}} = P(E_0 \cap (E_1|\bar{E}_2)), \tag{5}$$

$$P_{\mathsf{DE}} = P(E_0 \cap (\bar{E}_1|E_2)), \tag{6}$$

where $\bar{E}_n$ represents the non-occurrence of the event E_n.

In order to calculate P_{FA} and P_{DE}, consider a network with two nodes A and B, with node A continuously transmitting PRSs, while node B either transmits a PRS or remains silent. To determine the detection error and the false alarm rate at node A, we view this scenario as an on-off keying (OOK) transmission, with node B transmitting 'bit 1' when it transmits a PRS, and 'bit 0' when it does not. Here, 'bit 1' corresponds to the PRS signal s_1, whose samples are given by [8]

$$s_1[\ell] = \frac{10^{3/20}}{\sqrt{L}} \sum_{c \in \mathscr{C}} \cos\left(\frac{2\pi \cdot c \cdot \ell}{L} - \psi(c)\right), \quad \ell = 0, 1, ..., L-1, \tag{7}$$

where L is the total number of time samples transmitted in the PRS signal, $\mathscr{C}$ is the set of orthogonal frequency division multiplexed (OFDM) sub-carriers used for PRS transmission, and $\psi(c)$ is a sub-carrier specific phase angle [8]. Thus, P_{FA} represents the probability of node A detecting a '1' when a '0' is transmitted by node B, and P_{DE} represents the probability of detecting a '0' when a '1' is transmitted. Considering that the signal is subject to possible phase distortions along the line, we apply non-coherent detection at node A. Under such a condition, P_{FA} and P_{DE} are the bit error probabilities of non-coherent OOK detection, and can be expressed as [27, Ch. 7]

$$P_{\mathsf{FA}} = \exp\left(-\frac{b_0^2}{2}\right), \tag{8}$$

$$P_{\mathsf{DE}} = 1 - \mathcal{Q}\left(\sqrt{2\gamma}, b_0\right), \tag{9}$$

where $\mathcal{Q}(\cdot,\cdot)$ is the first-order Marcum-Q function, b_0 is the decision threshold of non-coherent OOK normalized to the root-mean-square noise value, and γ is the signal-to-noise ratio (SNR). The latter is given as

$$\gamma = \frac{E_{\mathrm{b}}}{N_0 + \Psi_{\mathsf{RSI}}}, \tag{10}$$

where E_{b} represents the received energy per-bit[2], N_0 is the average power spectral density (PSD) of the cumulative noise at the receiver of node A, and Ψ_{RSI} is the average residual self-interference (RSI) PSD after non-ideal self-interference cancellation. For brevity, we define $N_{0,\mathrm{FD}} = N_0 + \Psi_{\mathsf{RSI}}$ as the new effective 'noise floor' under IBFD operation.

To determine realistic values of P_{DE} and P_{FA} in a HAN, we derive an expression for γ in terms of known transmission parameters and channel conditions. The received bit-energy can be written as $E_{\mathrm{b}} = \Phi_{\mathrm{R}} t_{\mathrm{pd}}$, where t_{pd} is the time interval for PRS detection, which is related to the PRS time t_{SLOT} as $t_{\mathrm{pd}} = t_{\mathrm{SLOT}} - 2t_{\mathrm{RI}}$, where t_{RI} is the roll-off time interval at the beginning and the end of a PRS and is not used for signal detection. On the other hand, Φ_{R} is the power of the received signal, which can in turn be written as

$$\Phi_{\mathrm{R}} = \int_{f_1}^{f_2} \Psi_{\mathrm{R}}(f) \mathrm{d}f, \tag{11}$$

with $\Psi_{\mathrm{R}}(f)$ being the PSD of the received signal at a frequency f, and f_1 and f_2 are the lower and upper frequency limits of the transmission band, respectively. We further express $\Psi_{\mathrm{R}}(f)$ in terms of the known transmit PSD, $\Psi_{\mathrm{T}}(f)$, as $\Psi_{\mathrm{R}}(f) = \Psi_{\mathrm{T}}(f) \cdot |H(f)|^2$, where $H(f)$ is the power line channel frequency response at frequency f from node B to node A. The maximum transmit PSD is typically regulated to limit the electromagnetic interference caused by BB-PLC [21]. For our analysis, we consider the devices to always transmit signals with maximum PSD $\Psi_{\mathrm{T,max}}$, although newer devices support variable transmit PSDs [28]. Further, it is safe to assume the channel gain to be flat within each sub-carrier, since the HPAV PRS sub-carrier spacing is smaller than the observed channel coherence bandwidth in typical in-home BB-PLC networks [8], [29]. We can therefore re-write (11) as

$$\Phi_{\mathrm{R}} = \Psi_{\mathrm{T,max}} \sum_{c \in \mathscr{C}} |H(f_c)|^2 \cdot \Delta f, \tag{12}$$

where f_c is the center frequency of the cth OFDM sub-carrier, and Δf is the sub-carrier spacing. Since $N_{0,\mathrm{FD}} = \frac{1}{|\mathscr{C}|} \sum_{c \in \mathscr{C}} N_{0,\mathrm{FD}}(f_c)$, where $N_{0,\mathrm{FD}}(f_c)$ is the effective noise floor of the cth OFDM sub-carrier under IBFD operation, we express (10) as

$$\gamma = \Psi_{\mathrm{T,max}} t_{\mathrm{pd}} \Delta f |\mathscr{C}| \frac{\sum_{c \in \mathscr{C}} |H(f_c)|^2}{\sum_{c \in \mathscr{C}} N_{0,\mathrm{FD}}(f_c)}. \tag{13}$$

We now determine the optimal value of the threshold b_0 to be used in (8) and (9). Denoting the overall network node error rate as

$$P_{\mathrm{e}} = P(E_2|E_0) P_{\mathsf{DE}} + P(\bar{E}_2|E_0) P_{\mathsf{FA}}, \tag{14}$$

we define the optimal threshold as

$$b_{\mathrm{opt}} \triangleq \arg\min_{b_0} \; P_{\mathrm{e}}. \tag{15}$$

In the appendix, we derive a closed-form approximation of the optimal threshold solution as

$$b_{\mathrm{opt}} \approx \widetilde{b}_{\mathrm{opt}} = \sqrt{\frac{(\gamma + \ln\tau)^2 + 4(\gamma + \ln\tau)}{2\gamma}}, \tag{16}$$

where $\tau = \frac{P(\bar{E}_2|E_0)}{P(E_2|E_0)}$. The value of τ at a given node depends on the transmitting priorities and the congestion conditions of other network nodes.

When a node transmits a PRS, i.e., when the event E_0 occurs, the other network nodes have a conditional probability of $P(\bar{E}_2|E_0)$ to not transmit any PRS, and $P(E_2|E_0)$ to

[2]The term 'bit' here refers to the PRS signal in one PRS slot used for signal detection.

transmit at least one. Thus, τ can be estimated locally at any given node by counting the number of priority resolution slots where at least one other node also transmits a PRS, while the considered node transmits a PRS itself. This can easily be achieved due to the IBFD operation applied at each network node. Such an estimation of τ relies on a local historical record of PRS detection. When this record is unavailable, such as during the bootstrapping of the network, the node sets $\tau = 1$ as in [1] to minimize $P_{\mathsf{FA}}+P_{\mathsf{DE}}$. This serves as an upper bound for both P_{FA} and P_{DE} individually and yields near-zero error rates as shown later in this section. The node then dynamically updates τ to minimize P_{e}.

Since P_{e} is a monotonically decreasing function with respect to γ for the optimum detection threshold b_{opt} (which is closely approximated by $\widetilde{b}_{\mathrm{opt}}$) [27, Ch. 7], and since $\frac{|H(f_c)|^2}{N_{0,\mathrm{FD}}(f_c)}$ decreases with $|H(f_c)|^2$ [10], we use the worst-case minimum channel gain, $|H_{\min}|^2$, across all sub-carriers to obtain an upper bound for the total error, P_{tot}, as

$$P_{\mathrm{tot}} = P_{\mathsf{DE}} + \tau P_{\mathsf{FA}} \tag{17}$$

$$\leq 1 - \mathcal{Q}\left(\sqrt{2\gamma_{\min}}, \widetilde{b}_{\mathrm{opt}}\right) + \tau \exp\left(-\frac{\widetilde{b}_{\mathrm{opt}}^2}{2}\right), \tag{18}$$

where $\gamma_{\min} = \dfrac{\Psi_{\mathrm{T,max}}|\mathscr{C}||H_{\min}|^2 \Delta f t_{\mathrm{pd}}}{N_{0,\mathrm{FD}}}$.

The only remaining unknown is $N_{0,\mathrm{FD}}$, which we determine by referring to [10, Table II] that reports the signal-to-canceled-interference-plus-noise-ratio (SCINR) after the self-interference cancellation under different channel conditions. We compute $N_{0,\mathrm{FD}}$ as

$$N_{0,\mathrm{FD}}(f) = \frac{\Psi_{\mathrm{R}}(f)}{\mathsf{SCINR}(f)}. \tag{19}$$

It has also been shown in [10] that $\mathsf{SCINR}(f)$ varies with changing $H(f)$. Since we consider a worst-case performance with $|H_{\min}|^2$, we calculate $N_{0,\mathrm{FD}}$ as

$$N_{0,\mathrm{FD}} = \frac{\Psi_{\mathrm{T,max}} \cdot |H_{\min}|^2}{\mathsf{SCINR}}, \tag{20}$$

where SCINR is the associated self-interference cancellation performance for $|H_{\min}|^2$.

We now calculate the values of $\gamma_{\min}$ that we obtain for different $|H_{\min}|^2$. In accordance with the HPAV specifications, we set $\Psi_{\mathrm{T,max}} = -50$ dBm/Hz, $\Delta f = 195$ kHz, $|\mathscr{C}| = 153$, and $t_{\mathrm{pd}} = 25.92$ μs [8]. The resulting $\gamma_{\min}$ values are listed in Table I. Next, we compute the associated $\widetilde{b}_{\mathrm{opt}}$. Finally, we use (18) to determine the practical upper-bound values of P_{tot} that we expect to encounter when CFP is deployed in in-home networks.

As an example, we consider the case where $\tau = 1$ to evaluate P_{tot}. With the values computed in Table I and using (16), we calculate P_{tot} to be near-zero ($< 10^{-100}$) under various minimum channel gain conditions down to $|H_{\min}|^2 = -60$ dB.

For other values of τ ranging between 0.01 and 100, we find P_{tot}, P_{FA}, and P_{DE} to all be nearly zero as well. This assures us that the deployment of CFP in practical in-home BB-PLC network environments results in virtually no detection errors or false alarms.

TABLE I
PRS SNR UNDER VARYING MINIMUM CHANNEL GAINS

$\lvert H_{\min}\rvert^2$ (dB)	SCINR (dB)	$N_{0,\mathrm{FD}}$ (dBm/Hz)	$\gamma_{\min}$ (dB)
-5	32	-87	60
-10	30	-90	58
-20	27	-97	56
-30	27	-107	56
-40	21	-111	50
-50	12	-112	40
-60	2	-112	30

D. Impact of PLC Noise

The performance of our proposed solution is entirely dependent on the self-interference cancellation ability of the IBFD solution used, and our solution is equally applicable under all PLC noise conditions. Under moderate to low noise scenarios, where Ψ_{RSI} is the more dominant component of $N_{0,\mathrm{FD}}$, the values presented in Table I remain unchanged as it is equivalent to the condition that we have reported our values for, i.e., with $N_0 = -120$ dBm/Hz and $N_{0,\mathrm{FD}} \geq -112$ dBm/Hz. On the other hand, when power line noise is the limiting factor of SCINR, i.e., when N_0 is the more dominant component of $N_{0,\mathrm{FD}}$, the values of $\gamma_{\min}$ are lower than those reported in Table I. However, note that such a condition is similar to a half-duplex (HD) signal detection and is not a result of IBFD detection. The PRS signals are designed in the HPAV standard with multiple repetitions in order to be resilient to harsh power line noise conditions. For example, with $\tau = 1$, and a power line noise as high as $N_0 = -103$ dBm/Hz on all sub-carriers, we still achieve a total error rate of $P_{\mathrm{tot}} = 10^{-20}$. The multiple PRS repetitions also enable an impulse noise resilient PRS signal detection. In addition, the impulse noise events occur with a low probability [30], [31].

Despite this, if a node is unable to detect a PRS signal sent by another network node, the adverse effects associated (such as, the two nodes being hidden from each other during the PRS transmission phase) are exactly the same as those in an HD case. Such conditions could potentially result in data payload collisions, just as it would in an HD operation. However, we do not address such collisions in this work. We focus on the more common cause of frame collisions resulting from two or more network nodes having the same value of BC. In the following section, we use the underlying technique built in Section III to design an MPD scheme to eliminate such collisions.

IV. MUTUAL PREAMBLE DETECTION

In this section, we introduce our second access control scheme called MPD, where we use the medium-aware transmission ability provided by the IBFD operation to avoid the lengthy collision recovery by predicting a future frame collision. Through MPD, we essentially propose a practical scheme to realize CSMA/CD in BB-PLC networks by detecting the overlapping preamble signals.

A. Network Operation with MPD

We enable all nodes in the network with the ability to transmit a preamble and simultaneously sense the power line medium for other possible preamble signal transmissions. In this way, when two or more network nodes transmit a preamble signal at the same back-off time slot and gain access to the power line channel simultaneously, they each predict a future data payload collision by detecting a preamble other than their own. Under such circumstances, we compel these conflicting nodes to transmit another preamble signal subsequently. This acts as a jamming signal to ensure that all network nodes are made aware of a potential collision. We then let the nodes follow the standard HPAV collision recovery procedure within an interval of t_{CIFS}. This operation is illustrated in Fig. 4.

We notice that the time interval between the two back-off stages (the back-off stage of the colliding MAC frame and the back-off stage after the collision recovery) is reduced to $t_{\mathrm{p}} + t_{\mathsf{CIFS}}$ with our MPD scheme, while it is of duration t_{EIFS} in the original HPAV MAC protocol, as shown in Fig. 2.

B. IBFD Preamble Detection

To determine the success of IBFD preamble detection, consider a BB-PLC network with two nodes, A and B, with node A continuously transmitting preambles slot-by-slot, while in each time slot, node B either transmits a preamble or not. Similar to Section III-C, we view the behavior of node B as a source continuously transmitting information bits using on-off keying, with the preamble signal being the transmission pulse. In every preamble time slot, node B transmits a bit '1' to send a preamble to node A, and a '0' when it has nothing to transmit. An IBFD enabled node A is able to continuously detect the information bit sent by node B in each time slot. This scenario is similar to the one considered in Section III-C, albeit, the transmission pulse is now a preamble signal, s_2, where

$$s_2[\ell] = \frac{10^{3/20}}{\sqrt{L}} \sum_{c \in \mathscr{C}} \cos\left(\frac{2\pi \cdot c \cdot \ell}{L} + \psi(c)\right), \quad \ell = 0, 1, ..., L-1, \qquad (21)$$

with the value of L being the same as that for the PRS signal. The preambles also use the same set of OFDM sub-carriers as the PRSs, with the phase shift of each corresponding sub-carrier being the same in magnitude but opposite in sign. Therefore, the P_{FA} and P_{DE} formulations in Section III-C also apply to the above scenario. This also implies that all the computations in (8)–(20), as well as the data reported in Table I, are valid for detecting preambles as well. Thus, the detection error rate and the false alarm rate for MPD are also practically zero.

V. Numerical Evaluations

In this section, we first describe the comprehensive simulation model we build to emulate a real HAN traffic. In particular, we enable multiple priority levels that are indicative of the heterogeneous nature of the HAN traffic. Further, we introduce the Poisson traffic shaping (PTS) to emulate a real HAN traffic arrival, and apply a network resource allocation scheme to ensure that each priority level acquires an appropriate share of the network resource. We then use both the classical simplistic model and the comprehensive model we built to present OMNeT++ simulation results of the CFP and MPD performances, to verify the effectiveness of our proposed schemes.

A. Network Traffic

The performance of a distributed coordinated network is often evaluated with the assumptions of a single-priority saturated network traffic [25], [26], [32]. However, such assumptions are not only not indicative of realistic in-home PLC networks, but they also limit our ability to test the effectiveness of our proposed schemes. For example, recall that a CFC is a condition where a single node wins the PRP among all contending nodes. With a single-priority saturated network traffic arrival, all the network nodes contend with the same priority level in each PRP, which never creates a CFC. On the other hand, network traffic in a typical HAN is heterogeneous in nature, which is well accommodated by the multiple priority levels of HPAV. Furthermore, a typical HAN consists of network traffic from both high-speed multimedia and smart home applications. While network traffic arrivals of the smart home applications are found to be well emulated by the Poisson process [33], [34], those of the multimedia applications are found to be self-similar in nature [35], and well emulated by a Markov-Modulated Poisson Process (MMPP) [36]. Thus, we build a comprehensive simulation model with multiple priority levels and PTS to generate a realistic network traffic condition. Since the performance with a single-priority saturated network traffic is also an important evaluation metric of MAC protocols, we use both the classical simplistic model and our comprehensive model for our network simulations.

B. Poisson Traffic Shaping

For simplicity, we emulate the network traffic arrivals of the multimedia applications with the 1-state MMPP, so that we can emulate the HAN traffic arrivals with the Poisson process as in [32]. The PTS adopted in our comprehensive model pushes the MAC frames according to the Poisson process [37], with a mean arrival rate of $\lambda_{n,i}$ at the nth network node for the ith priority MAC frame ($i \in \{1, 2, 3\}$). Note that we do not shape data packets with priority 0. When all the higher priority messages are successfully transmitted by the node, it attempts to transmit a best-effort data frame of priority 0.

C. Network Resource Allocation

Recall from Section II-A that the PRP ensures messages of higher priority levels always get transmitted before those of lower priority levels. However, this has been shown, in [38], to result in lower priority starvation when the network traffic of higher priority levels gets saturated. Therefore, to enable a heterogeneous network traffic with multiple priority levels, and to ensure a minimum bandwidth guarantee for the lower

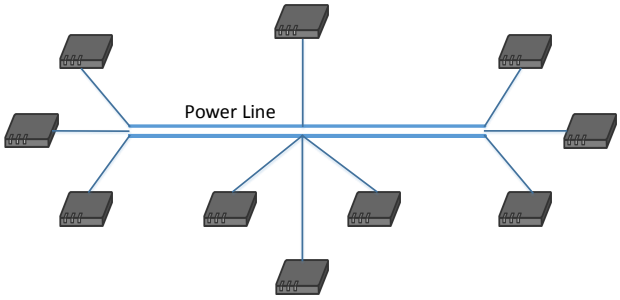

Fig. 5. In-home BB-PLC network simulation topology.

priority frames, our comprehensive model allocates an appropriate share of the network resource to each priority level, beyond the conventional PRP of the HPAV protocol.

We denote the average MAC frame intervals at the nth network node as $\mu_{n,i}$ for the ith priority MAC frame ($i \in \{1,2,3\}$). This can be seen in Fig. 1 as the duration from the beginning of the PRS_0 to the end of the CIFS. For a network with N active network nodes, we ensure that

$$\sum_{n=1}^{N}(\mu_{n,3}\lambda_{n,3} + \mu_{n,2}\lambda_{n,2} + \mu_{n,1}\lambda_{n,1}) = \kappa, \qquad (22)$$

where $\kappa < 1$. We choose κ by accounting for a fair portion of the network resource to be reserved for collisions and retransmissions. The remaining network resource is utilized for best effort message transmission. This guarantees that every ith ($i \neq 0$) priority level gets an appropriate share of the network resource, $\kappa_i = \sum_{n=1}^{N} \mu_{n,i}\lambda_{n,i}$.

D. Simulation Configuration

We use a discrete event simulator, OMNeT++, to simulate the in-home PLC network [39]. A set of $\mathcal{N}$ nodes are interconnected to each other through the power line medium to form a fully meshed network, as shown in Fig. 5. In our simulations, we assume an identical time interval of the data payload, t_{FL}, regardless of its priority level. Further, we do not consider the MAC frame retransmissions associated with transmission errors in data payloads as they do not affect η as defined in (2). We enlist all simulation parameters in Table II, which are based on the HPAV specifications [8]. The statistical significance of the simulation results is guaranteed by the sufficient duration of each simulation run, T_{S}, where the resultant MAC efficiency is the average performance of several thousands of MAC frame transmissions.

By denoting the total number of collision-free MAC frames transmitted as n_{T}, we compute η at the end of each simulation run as

$$\eta = \frac{n_{\text{T}} t_{\mathsf{FL}}}{T_{\text{S}}}. \qquad (23)$$

E. Performance of CFP with Single Node Flooding

For our first result, we use the following network setting to test the effectiveness of the CFP scheme. We set $|\mathcal{N}| = 1$ by letting a single node be the only active network node that continuously transmits priority-3 MAC frames to all the other network nodes without channel idling. Under such a scenario, our proposed MPD scheme has no effect as no contentions or collisions occur with this setting. The impact of varying t_{FL} on the achieved MAC efficiency with and without CFP is shown in Fig. 6.

TABLE II
SIMULATION PARAMETERS

Parameter	Value
Simulation time, T_{S}	30 s
t_{CIFS}	100 μs
PRS and Back-off slot time, t_{SLOT}	35.84 μs
t_{P}	35.84 μs
t_{FC}	133.92 μs
MaxFL	2341.12 μs
t_{RIFS}	140 μs
t_{EIFS}	2920.64 μs

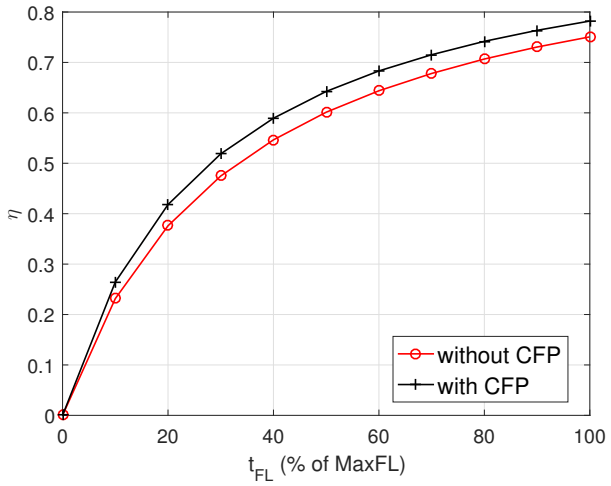

Fig. 6. MAC efficiency as a function of t_{FL} with single node flooding.

Since the network experiences no collision or idle time intervals, the power line medium is kept busy by continuously transmitting MAC frames shown in Fig. 1. Under such conditions we refer to (1) and express the MAC efficiency as

$$\eta = \frac{t_{\mathsf{FL}}}{(t_{\mathsf{EIFS}} - \mathsf{MaxFL}) + t_{\mathsf{FL}} + (2 + \mathbb{E}[n_{\text{BF}}])t_{\text{SLOT}}}, \qquad (24)$$

where $\mathbb{E}[n_{\text{BF}}]$ is the expected number of back-off time slots. The absence of contentions and collisions contains the contention at the base stage, which provides $\mathbb{E}[n_{\text{BF}}] = \frac{\mathsf{CW}_{\min}}{2}$ for the original HPAV protocol, where $\mathsf{CW}_{\min}$ is the minimum contention window. However, with our CFP deployed, the transmitting node detects a CFC at every frame transmission, which results in $\mathbb{E}[n_{\text{BF}}] = 0$, thereby increasing η. We can also observe in Fig. 6 that the maximum MAC efficiency shown in (3) is achieved when $t_{\mathsf{FL}} = \mathsf{MaxFL}$.

F. Performance Evaluations with Multiple Active Nodes

For our next set of results, we run our simulations with multiple active nodes under both, the classical simplistic network traffic model and the comprehensive model described in Section V-A. We form two sub-settings where we fix $|\mathcal{N}| = 10$ and vary t_{FL} in the first case, while we fix $t_{\mathsf{FL}} = \mathsf{MaxFL}$ and vary $|\mathcal{N}|$ in the second.

Network Resource Allocation in our Comprehensive Model: We estimate the average MAC frame interval at the nth network node in our simulations as

$$\mu_{n,i} \approx \mu = (t_{\mathsf{EIFS}} - \mathsf{MaxFL}) + t_{\mathsf{FL}} + 2t_{\mathrm{SLOT}}. \tag{25}$$

We can then rewrite (22) as

$$\mu \sum_{n=1}^{|\mathcal{N}|} (\lambda_{n,3} + \lambda_{n,2} + \lambda_{n,1}) = \kappa. \tag{26}$$

To account for the back-off time slots we ignored in our approximation of (25), we choose a smaller $\kappa = 0.65$. By setting $\sum_{n=1}^{|\mathcal{N}|} \lambda_{n,i} = \frac{\kappa_i}{\mu}$, the comprehensive model allocates a certain portion of network resource to the ith priority network traffic, which for simplicity, is further allotted equally to all $|\mathcal{N}|$ network nodes. Thus, we have $\lambda_{n,i} = \frac{1}{|\mathcal{N}|}\frac{\kappa_i}{\mu}$, $\forall n \in \mathcal{N}$ and $i \in \{1, 2, 3\}$. In our simulations, we set $\kappa_3 = 0.25$, and $\kappa_2 = \kappa_1 = 0.2$.

1) Varying t_{FL}: We first simulate the network with varying t_{FL} and fix $|\mathcal{N}| = 10$. The variation of the MAC efficiency with varying t_{FL} under the two network traffic models is shown in Fig. 7. The curves essentially resemble those in single node flooding, but with reduced η in both traffic scenarios, because of contentions and collisions. More specifically, we observe in the results for the saturated network traffic that the MAC efficiency is significantly degraded due to the large number of contentions and collisions caused by the constant frame transmissions of all network nodes. However, our MPD scheme successfully improves the MAC efficiency such that the obtained η with $|\mathcal{N}| = 10$ essentially matches that of the single-node flooding case. We further notice that while the performance enhancements provided by MPD can be observed in both network traffic models, the introduction of CFP shows no improvements with the simplistic model as saturated single-priority data arrival produces no CFCs.

We observe that under a realistic HAN traffic scenario, simultaneous deployment of CFP and MPD with $t_{\mathsf{FL}} = \mathsf{MaxFL}$ yields an $\eta = 76.80\%$, which achieves 98.16% of the optimal MAC efficiency, $\max(\eta) = 78.24\%$. Under the same conditions, a conventional HPAV protocol only manages to provide $\eta = 69.43\%$, which is further reduced to $\eta = 54.37\%$ under a saturated network scenario.

2) Varying Active Nodes: For our final result, we simulate the network with varying $|\mathcal{N}|$ and a fixed $t_{\mathsf{FL}} = \mathsf{MaxFL}$. The simulation results of this sub-setting under the two network traffic models are shown in Fig. 8. We observe that without our MPD scheme, η decreases as the number of active network nodes increases in both the network traffic models, due to the increased collision rate as well as the lengthy collision recovery time. However, we achieve a stable η across different number of nodes using our MPD scheme, which is attributed to the reduced collision recovery time. Similar to the results seen in Fig. 7, we see no improvements due to CFP with the saturated network traffic model while the improvements are clearly visible under the comprehensive simulation model. We observe that we obtain the greatest η, both in terms of absolute value and stability across increasing nodes, using both our proposed schemes of CFP and MPD under a realistic network traffic scenario.

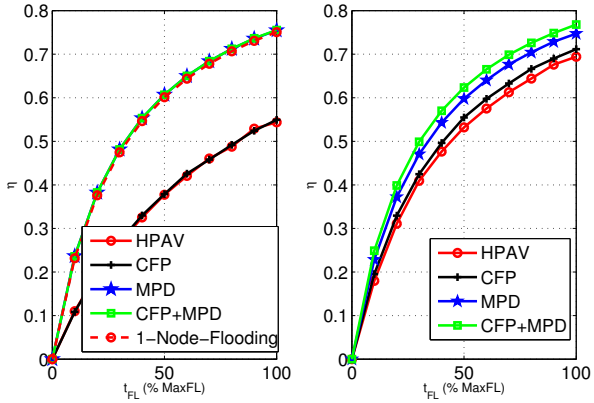

Fig. 7. MAC efficiency as a function of t_{FL} for the classical simplistic traffic model (left) and the comprehensive multiple priority PTS model (right).

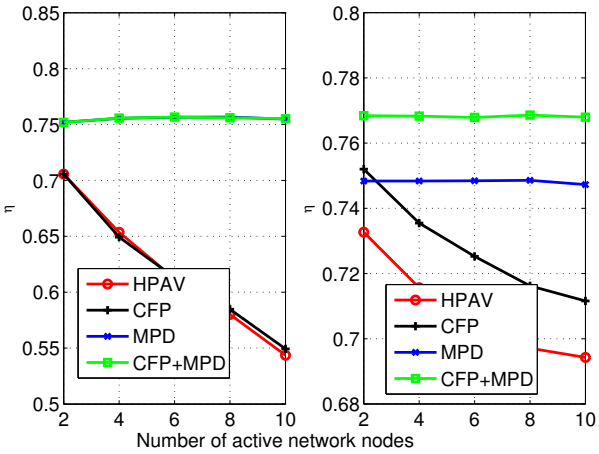

Fig. 8. MAC efficiency as a function of the number of active nodes for the classical simplistic traffic model (left) and the comprehensive multiple priority PTS model (right).

VI. Deployment of CFP and MPD on a BB-PLC Device

A. Hardware Implementation Costs

The elementary requirement for implementing CFP and MPD in power line networks is to enable BB-PLC modems with the IBFD operation. Recent works have shown that an IBFD implementation on legacy BB-PLC devices requires minimal changes to the modem chip-sets, with only an addi-

tional power consumption of about 0.1 W for the active hybrid circuit that is used at the power line-modem interface [18].

B. Interoperability

Our proposed CFP and MPD schemes are completely interoperable with HD devices. With the CFP scheme, an IBFD-enabled node can detect a CFC when it is the only node transmitting the highest priority message regardless of whether the other nodes are IBFD-enabled. However, such an HD node is unable to detect a CFC. On the other hand, the MPD technique still offers improvements in η when only a part of the network nodes are IBFD-enabled, but with reduced effect compared to the case when all the network nodes are IBFD-enabled. As long as the conflicting nodes are IBFD-enabled, a data payload collision can be successfully predicted and avoided using MPD. However, when an HD node is involved as a conflicting node, the ensuing data payload collision is inevitable, and it takes the network a time interval of EIFS to recover from it.

VII. Conclusion

In this paper, we have leveraged the medium-aware transmission enabled by IBFD to propose two novel schemes called CFP and MPD to improve the MAC efficiency of a standard HPAV protocol. Specifically, we proposed CFP to eliminate the redundant back-off stages by IBFD detection of the PRSs, and MPD to avoid the lengthy collision recovery by IBFD detection of the preamble signals. By adopting realistic self-interference cancellation performance reported in IBFD BB-PLC systems, our analytical results suggest that both CFP and MPD work with virtually no detection errors or false alarms. Further, we have developed a comprehensive simulation model to evaluate the performance of our proposed schemes as a supplement to the classical simplistic network traffic scenario. Our simulation results have shown that both our proposed schemes provide considerable improvement in MAC efficiency when applied independently, and further improve the efficiency significantly when used together.

Appendix

Optimal Detection Threshold and its Closed-Form Approximation

In this appendix, we derive an analytical expression and a closed-form approximation for the optimum detection threshold, $b_{\rm opt}$, by solving (15).

A. Optimal Detection Threshold

We start with (14), and divide both sides by $P(E_2|E_0)$ to get

$$P_\tau = \frac{P_{\rm e}}{P(E_2|E_0)} = P_{\mathsf{DE}} + \tau P_{\mathsf{FA}}, \tag{27}$$

where $\tau = \frac{P(\bar{E}_2|E_0)}{P(E_2|E_0)}$. Since $P(E_2|E_0)$ is a constant for a given network operation, minimizing (27) also solves (15). To derive the optimum detection threshold that minimizes (27), we study the derivative of P_τ with respect to the normalized decision threshold b_0, which can be expressed as

$$D(b_0) = \frac{\partial P_{\mathsf{DE}}}{\partial b_0} + \tau \frac{\partial P_{\mathsf{FA}}}{\partial b_0}. \tag{28}$$

We first individually find the partial derivatives of both the components of P_τ using (8) and (9) to get

$$\frac{\partial P_{\mathsf{FA}}}{\partial b_0} = -b_0 \exp\left(-\frac{b_0^2}{2}\right), \tag{29}$$

$$\begin{aligned}\frac{\partial P_{\mathsf{DE}}}{\partial b_0} &= \frac{\partial}{\partial b_0}\left(1 - \int_{b_0}^{\infty} x \exp\left(-\frac{x^2+2\gamma}{2}\right) I_0\left(x\sqrt{2\gamma}\right) \mathrm{d}x\right) \\ &= \exp\left(-\frac{2\gamma + b_0^2}{2}\right) I_0\left(b_0\sqrt{2\gamma}\right) b_0,\end{aligned} \tag{30}$$

where $I_n(\cdot)$ is the nth-order modified Bessel function of the first kind. Therefore,

$$\begin{aligned}D(b_0) &= b_0 \exp\left(-\frac{b_0^2}{2}\right)\left(-\tau + \exp(-\gamma) I_0\left(b_0\sqrt{2\gamma}\right)\right) \\ &= f(b_0) D_{\rm N}(b_0),\end{aligned} \tag{31}$$

where $f(b_0) = b_0 \exp(-\frac{b_0^2}{2})$, and

$$D_{\rm N}(b_0) = -\tau + \exp(-\gamma) I_0(b_0\sqrt{2\gamma}). \tag{32}$$

Since b_0 is the normalized threshold of the signal energy for non-coherent OOK detection, it can only take non-negative values. Thus, we only study $\mathrm{sgn}\left(D(b_0)\right)$ for $b_0 \geq 0$, where $\mathrm{sgn}(\cdot)$ is the signum function [40, Ch. 6].

For $b_0 = 0$, it is easily observable that $\mathrm{sgn}\left(D(b_0)\right) = 0$. For the cases of $b_0 > 0$, we note that

$$\mathrm{sgn}\left(D(b_0)\right) = \mathrm{sgn}\left(D_{\rm N}(b_0)\right), \tag{33}$$

as $f(b_0) > 0$. Since $I_0(\cdot)$ is a monotonically increasing function, we conclude from (32) that $D_{\rm N}(b_0)$ also monotonically increases with b_0 for a given γ. Thus, the values of $\lim_{b_0 \to 0^+} D_{\rm N}(b_0)$ and $\lim_{b_0 \to +\infty} D_{\rm N}(b_0)$ reveal the exact nature of $\mathrm{sgn}\left(D_{\rm N}(b_0)\right)$ for $b_0 > 0$.

We first obtain the limit

$$\begin{aligned}\lim_{b_0 \to 0^+} D_{\rm N}(b_0) &= -\tau + \exp(-\gamma) \lim_{b_0 \to 0^+} I_0(b_0\sqrt{2\gamma}) \\ &= -\tau + \exp(-\gamma).\end{aligned} \tag{34}$$

By referring to Table I, we find that for various minimum power line channel gain conditions, γ is large enough to ensure that $\tau \exp(\gamma) > 1$ for practically operable values of τ. Therefore,

$$\lim_{b_0 \to 0^+} D_{\rm N}(b_0) < 0. \tag{35}$$

Next, we have

$$\begin{aligned}\lim_{b_0 \to +\infty} D_{\rm N}(b_0) &= -\tau + \exp(-\gamma) \lim_{b_0 \to +\infty} I_0(b_0\sqrt{2\gamma}) \\ &= -\tau + \exp(-\gamma) I_0(\sqrt{2\gamma} \lim_{b_0 \to +\infty} b_0) \\ &= +\infty.\end{aligned} \tag{36}$$

With (35), (36) and the monotonicity of $D_{\rm N}(b_0)$, we can deduce that there exists a unique positive zero-point $b_{\rm zp} > 0$, such that

$$\operatorname{sgn}(D_{\rm N}(b_0)) = \begin{cases} -1, & 0 < b_0 < b_{\rm zp} \\ 0, & b_0 = b_{\rm zp} \\ +1, & b_0 > b_{\rm zp}. \end{cases} \tag{37}$$

Therefore, from (33) and (37), we conclude

$$b_{\rm opt} = b_{\rm zp}. \tag{38}$$

Since $b_{\rm zp}$ is the solution to the differential equation $D(b_0) = 0$, we get

$$\exp(-\gamma) I_0\left(b_{\rm opt}\sqrt{2\gamma}\right) = \tau. \tag{39}$$

$$\implies b_{\rm opt} = \frac{I_0^-(\tau \exp(\gamma))}{\sqrt{2\gamma}}, \tag{40}$$

where $I_n^-(\cdot)$ is the inverse of nth-order modified Bessel function of the first kind.

B. Closed-form Approximation

Finally, we derive a closed-form approximation of (40) for the purposes of practical implementation. To this end, we use the proven result that $b = \sqrt{2 + \frac{\gamma}{2}}$ provides an excellent analytic approximation to the solution of $\exp(-\gamma) I_0\left(b\sqrt{2\gamma}\right) = 1$ [27, Eqns. 7-4-13, 7-4-14, Fig. 7-4-3]. Thus, we have

$$\exp(\gamma) \approx I_0\left(\sqrt{\gamma(\gamma+4)}\right)$$

$$\implies I_0\left(b_{\rm opt}\sqrt{2\gamma}\right) \approx \exp\left(\sqrt{2b_{\rm opt}^2\gamma + 4} - 2\right). \tag{41}$$

Using (41) in (39), and simplifying with some simple manipulations gives us the closed-form approximation for $b_{\rm opt}$ as

$$b_{\rm opt} \approx \widetilde{b}_{\rm opt} = \sqrt{\frac{(\gamma + \ln\tau)^2 + 4(\gamma + \ln\tau)}{2\gamma}}. \tag{42}$$

REFERENCES

[1] Y. Huo, G. Prasad, L. Lampe, and V. Leung, "Mutual preamble detection for full duplex broadband power line communications," in *IEEE Global Communications Conf. (GLOBECOM)*, pp. 1–6, December 2016.

[2] L. Lampe, A. Tonello, and T. Swart, "Introduction," in *Power Line Communications: Principles, Standards and Applications From Multimedia to Smart Grid* (L. Lampe, A. Tonello, and T. Swart, eds.), ch. 1, pp. 1 – 7, John Wiley and Sons Ltd, 2016.

[3] S. Nowak, F.-M. Schaefer, M. Brzozowski, R. Kraemer, and R. Kays, "Towards a convergent digital home network infrastructure," *IEEE Trans. Consum. Electron.*, vol. 57, no. 4, pp. 1695–1703, 2011.

[4] "HomePlug 1.0 specifications," *HomePlug Powerline Alliance*, June 2001.

[5] S. Galli, H. Latchman, V. Oksman, G. Prasad, and L. Yonge, "Multimedia PLC systems," in *Power Line Communications: Principles, Standards and Applications From Multimedia to Smart Grid* (L. Lampe, A. Tonello, and T. Swart, eds.), ch. 8, pp. 475 – 511, John Wiley and Sons Ltd, 2016.

[6] J.-P. Javaudin and M. Bellec, "Omega project: On convergent digital home networks," in *IEEE 3rd Int. Workshop Cross Layer Design (IWCLD)*, pp. 1–5, 2011.

[7] A. Nayagam, P. Rajkotia, M. Krishnam, M. Rindchen, M. Stephan, and D. Rende, "IEEE 1901: Broadband over power line networks," in *MIMO Power Line Communications: Narrow and Broadband Standards, EMC, and Advanced Processing* (L. T. Berger, A. Schwager, P. Pagani, and D. Schneider, eds.), ch. 13, pp. 357 – 390, CRC Press, 2014.

[8] "HomePlug AV specification," *HomePlug Powerline Alliance*, 2007.

[9] H. Hrasnica, A. Haidine, and R. Lehnert, *Broadband Powerline Communications: Network Design*. John Wiley & Sons, 2005.

[10] G. Prasad, L. Lampe, and S. Shekhar, "Enhancing transmission efficiency of broadband PLC systems with in-band full duplexing," in *IEEE Int. Symp. Power Line Communications and its Applications (ISPLC)*, March 2016.

[11] Y. Liao, K. Bian, L. Song, and Z. Han, "Full-duplex MAC protocol design and analysis," *IEEE Commun. Lett.*, vol. 19, no. 7, pp. 1185–1188, 2015.

[12] L. Song, Y. Liao, K. Bian, L. Song, and Z. Han, "Cross-layer protocol design for CSMA/CD in full-duplex wifi networks," *IEEE Commun. Lett.*, vol. 20, no. 4, pp. 792–795, 2016.

[13] A. Leon-Garcia and I. Widjaja, *Communication Networks*. McGraw-Hill Inc., 2003.

[14] S. Sen, R. R. Choudhury, and S. Nelakuditi, "CSMA/CN: carrier sense multiple access with collision notification," *IEEE/ACM Trans. Netw.*, vol. 20, no. 2, pp. 544–556, 2012.

[15] T. Vermeulen, F. Rosas, M. Verhelst, and S. Pollin, "Performance analysis of in-band full duplex collision and interference detection in dense networks," in *IEEE Annu. Consumer Communications & Networking Conf. (CCNC)*, pp. 595–601, 2016.

[16] Y.-S. Choi and H. Shirani-Mehr, "Simultaneous transmission and reception: Algorithm, design and system level performance," *IEEE Trans. Wireless Commun.*, vol. 12, no. 12, pp. 5992–6010, 2013.

[17] T. Vermeulen and S. Pollin, "Energy-delay analysis of full duplex wireless communication for sensor networks," in *IEEE Global Communications Conf. (GLOBECOM)*, pp. 455–460, 2014.

[18] G. Prasad, L. Lampe, and S. Shekhar, "In-band full duplex broadband power line communications," *IEEE Trans. Commun.*, vol. 64, pp. 3915–3931, Sept 2016.

[19] "IEEE standard for broadband over power line networks: Medium access control and physical layer specifications," *IEEE Std 1901-2010*, pp. 1–1586, Dec 2010.

[20] L. T. Berger, A. Schwager, P. Pagani, and D. Schneider, *MIMO Power Line Communications: Narrow and Broadband Standards, EMC, and Advanced Processing*. CRC Press, 2014.

[21] H. A. Latchman, S. Katar, L. Yonge, and S. Gavette, *Homeplug AV and IEEE 1901: A Handbook for PLC Designers and Users*. Wiley-IEEE Press, 2013.

[22] I. Tsokalo, G. Prasad, S. Mudriievskyi, and R. Lehnert, "CSMA/CD in PLC: Test with full G. hn and IP/UDP protocol stack," in *IEEE Int. Symp. Power Line Communications and its Applications (ISPLC)*, pp. 1–6, 2017.

[23] C. Vlachou, A. Banchs, J. Herzen, and P. Thiran, "On the MAC for power-line communications: Modeling assumptions and performance tradeoffs," in *IEEE Int. Conf. Network Protocols (ICNP)*, pp. 456–467, 2014.

[24] E. Kriminger and H. Latchman, "Markov chain model of HomePlug CSMA MAC for determining optimal fixed contention window size," in *IEEE Int. Symp. Power Line Communications and its Applications (ISPLC)*, pp. 399–404, 2011.

[25] C. Vlachou, A. Banchs, P. Salvador, J. Herzen, and P. Thiran, "Analysis and enhancement of CSMA/CA with deferral in power-line communications," *IEEE J. Sel. Areas Commun.*, vol. 34, no. 7, pp. 1978–1991, 2016.

[26] G. Bianchi, "Performance analysis of the IEEE 802.11 distributed coordination function," *IEEE J. Sel. Areas Commun.*, vol. 18, no. 3, pp. 535–547, 2000.

[27] M. Schwartz, W. R. Bennett, and S. Stein, *Communication Systems and Techniques*. John Wiley & Sons, 1995.

[28] L. Yonge, J. Abad, K. Afkhamie, L. Guerrieri, S. Katar, H. Lioe, P. Pagani, R. Riva, D. M. Schneider, and A. Schwager, "An overview of the HomePlug AV2 technology," *J. Electr. Comput. Eng.*, vol. 2013, 2013.

[29] F. J. Canete, J. Cortés, L. Díez, and J. T. Entrambasaguas, "A channel model proposal for indoor power line communications," *IEEE Commun. Mag.*, vol. 49, no. 12, pp. 166–174, 2011.

[30] J. A. Cortés, L. Diez, F. J. Canete, and J. J. Sanchez-Martinez, "Analysis of the indoor broadband power-line noise scenario," *IEEE Trans. Electromag. Compat.*, vol. 52, no. 4, pp. 849–858, 2010.

[31] G. Prasad, H. Ma, M. J. Rahman, F. Aalamifar, and L. Lampe, "A cumulative power line noise generator," 2016. [Online] Available: http://www.ece.ubc.ca/~gauthamp/PLCnoise.

[32] M. Y. Chung, M.-H. Jung, T.-J. Lee, and Y. Lee, "Performance analysis of HomePlug 1.0 MAC with CSMA/CA," *IEEE J. Sel. Areas Commun.*, vol. 24, no. 7, pp. 1411–1420, 2006.

[33] M. Laner, P. Svoboda, N. Nikaein, and M. Rupp, "Traffic models for machine type communications," in *Int. Symp. Wireless Communication Systems (ISWCS)*, pp. 1–5, VDE, 2013.
[34] S. W. Lai, G. G. Messier, H. Zareipour, and C. H. Wai, "Wireless network performance for residential demand-side participation," in *IEEE Innovative Smart Grid Technologies Conf. Europe (ISGT Europe)*, pp. 1–4, 2010.
[35] Z. Sahinoglu and S. Tekinay, "On multimedia networks: Self-similar traffic and network performance," *IEEE Commun. Mag.*, vol. 37, no. 1, pp. 48–52, 1999.
[36] T. Yoshihara, S. Kasahara, and Y. Takahashi, "Practical time-scale fitting of self-similar traffic with Markov-modulated Poisson process," *Telecommunication Systems*, vol. 17, no. 1, pp. 185–211, 2001.
[37] F. P. Kelly, "Networks of queues," *Advances in Applied Probability*, pp. 416–432, 1976.
[38] C. Cano and D. Malone, "When priority resolution goes way too far: An experimental evaluation in PLC networks," in *IEEE Int. Conf. Communications (ICC), London, UK*, pp. 952–957, June 2015.
[39] A. Varga, "OMNeT++," in *Modeling and Tools for Network Simulation*, pp. 35–59, Springer, 2010.
[40] R. Kories and H. Schmidt-Walter, *Electrical Engineering: A Pocket Reference*. Springer Science & Business Media, 2011.